Modulation of the Conductance-Voltage Relationship of the BK_{Ca} Channel by Shortening the Cytosolic Loop Connecting Two RCK Domains

Ju-Ho Lee,[†] Hyun-Ju Kim,[†‡] Hae-Deun Kim,[†] Byoung-Cheol Lee,[†‡§] Jang-Soo Chun,[†§] and Chul-Seung Park[†‡§*]
[†]Department of Life Science, [‡]Center for Distributed Sensor Network, and [§]Cell Dynamics Research Center, Gwangju Institute of Science and Technology, Gwangju, Korea

ABSTRACT Calcium-dependent gating of large-conductance calcium-activated potassium (BK_{Ca}) channels is mediated by the intracellular carboxyl terminus, which contains two domains of regulator of K^+ conductance (RCK). In mammalian BK_{Ca} channels, the two RCK domains are separated by a protein segment of 101 residues that is poorly conserved in evolution and predicted to have no regular secondary structures. We investigated the functional importance of this loop using a series of deletion mutations. We found that the length, rather than the specific sequence at the central region of the segment, is critical for the functionality of the channel. As the length of the loop is progressively shorted, the conductance-voltage relationship gradually shifts toward more positive voltages with a minimum length of 70 amino acids, in an apparent response to increased tension within the loop. Thus, the functional activity of the BK_{Ca} channel can be modulated by altering the tension of this loop region.

INTRODUCTION

Large-conductance calcium-activated potassium (BK_{Ca}) channels are activated synergistically by membrane depolarization and an increase in intracellular Ca^{2+} (1–4). By coupling chemical and electrical signals, these channels play important roles in modulating a number of physiological processes, such as neuronal excitability, smooth-muscle contraction, frequency tuning of hair cells, and immunity (5–9). BK_{Ca} channels are composed of two different subunits: the pore-forming α-subunit (Slowpoke1 or Slo1) and auxiliary β-subunits (10). Functional channels can be assembled as either homotetramers comprised of only α-subunits, or heterooctamers made up of α- and β-subunits. The α-subunit contains seven transmembrane (TM) segments and a long cytosolic carboxyl terminus (Fig. 1 *A*). A pore-forming region and a K^+-selective filter are located between the fifth and sixth segments (S5-S6) (11). Membrane depolarization and calcium binding differentially activate BK_{Ca} channels via separate regions of the α-subunit (12–14). Whereas positive charges on the fourth TM domain (S4) are responsible for sensing membrane voltage (15–19), calcium-dependent activation of the channel is mediated by the bulky carboxyl terminus, which contains two regulator of K^+ conductance (RCK) domains in tandem (20–22) and the Ca^{2+} bowl (14,23). The first RCK domain (RCK1), located at the proximal C-terminus of the Slo1 protein, contains two divalent-cation binding sites with high and low affinity for Ca^{2+}, respectively (25,26). The second domain (RCK2) is located in the distal region of the C-terminus and is immediately followed by the Ca^{2+} bowl, a high-affinity Ca^{2+}-binding site (22,27–29).

Based on the structure of an archaeal Ca^{2+}-activated K^+ channel, MthK, eight RCK domains (two per α-subunit) have been proposed to form a ''gating ring'' that transduces Ca^{2+} binding into opening of the channel pore (21,22,30). In analogy to the MthK channel, one can envision that the octameric gating ring of mammalian BK_{Ca} channel may expand when Ca^{2+} binds to putative high-affinity divalent cation sensors in RCK1 and the Ca^{2+} bowl (21,30,31). This ligand binding then facilitates opening of the channel gate, perhaps by increasing the tension on the spring-like linker segment between the gate and the RCK domains (32). Recently, it was reported that hydrophobic interaction between RCK1 and RCK2 is essential for Ca^{2+}-dependent activation of the channel (28). This interaction is reminiscent of the assembly (or fixed) interface between the two RCK domains within the gating ring of MthK (21,30). It was also proposed that the first loop of RCK2 is a part of the flexible interface that mediates conformational coupling between RCK1 and RCK2 (33). The two RCK domains are linked by a protein segment (Fig. 1 *A*). This connecting loop region is poorly conserved in evolution (Fig. 1 *B*) and is predicted to have no regular secondary structures (NORS). In an attempt to understand the functional importance of this segment, we constructed a series of deletion mutations within the linker region and investigated the mutational effects on channel activity in a heterologous system. We found that the length, rather than the specific sequence of the segment, is critical for the functionality of the channel. As the lengths of the loop were progressively shortened, the conductance-voltage relationship shifted to more positive voltages, with a minimum functional length of 70 amino acids.

MATERIALS AND METHODS

Expression of Slo1 channels in Chinese hamster ovary K1 cells

All electrophysiological experiments were performed on Chinese hamster ovary (CHO)-K1 cells expressing either the wild-type (WT) or mutant

Submitted October 20, 2008, and accepted for publication April 24, 2009.

*Correspondence: cspark@gist.ac.kr

Editor: Richard W. Aldrich.

0006-3495/09/08/0730/8 $2.00

doi: 10.1016/j.bpj.2009.04.058

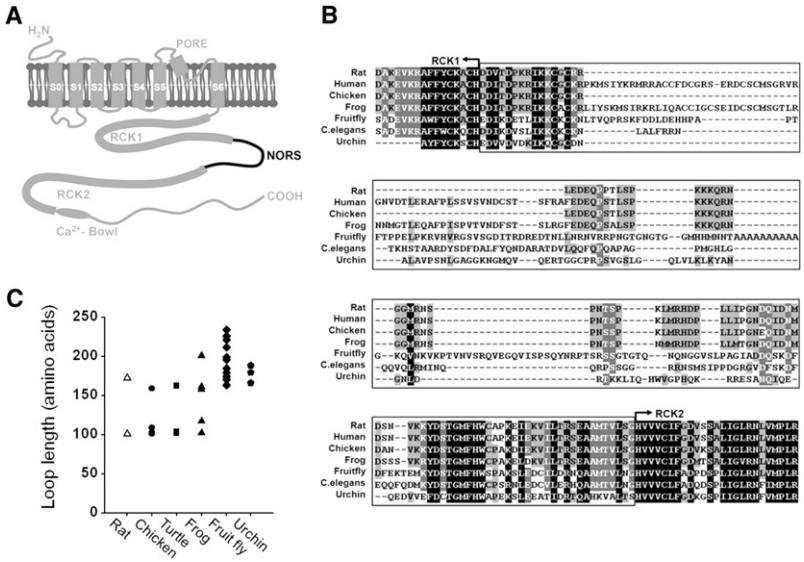

FIGURE 1 Comparison of the loop connecting RCK1 and RCK2 in BK_{Ca} channels of different organisms. (*A*) Membrane topology and schematic illustration of BK_{Ca} channel α-subunit (Slo1). The membrane-spanning regions and the cytoplasmic domain containing RCK1, RCK2, and the Ca^{2+} bowl are indicated. NORS represents the loop connecting RCK1 and RCK2 that is predicted to have no regular secondary structures. (*B*) Sequence alignment of the NORS regions between RCK1 and RCK2 in various organisms. Partial sequences of Slo1 channels from *Rattus norvegicus* (rat), *Homo sapiens* (human), *Gallus gallus* (chicken), *Xenopus laevis* (frog), *Drosophila melanogaster* (fruitfly), *Strongylocentrotus purpuratus* (sea urchin), and *Caenorhabditis elegans* (nematode) were aligned using ClusterX. (*C*) Diverse lengths of the NORS region among different isoforms of Slo1 in various species.

channels of the rat *Slo1* gene, *rSlo1* (GenBank accession number AF135265) (34). CHO-K1 cells were maintained in F-12K nutrient mixture, Kaighn's modification (Invitrogen, Carlsbad, CA), supplemented with 10% fetal bovine serum (Invitrogen) in a humidified atmosphere of 5% CO_2 at 37°C. To obtain high-quality plasmid DNA for transient transfection, the plasmid DNA was prepared using a commercial kit (Qiagen, Valencia, CA). Subconfluent monolayer cells on 35 mm plates were transfected in serum- and antibiotics-free media with 1.5 μg of total DNA using Polyfect transfection reagent (Qiagen). To identify transfected cells, we cotransfected *rSlo1*/pcDNA3.1 with pEGFP (Invitrogen) at a molar ratio of 10:1. We monitored EGFP signals using an Olympus IX51 microscope.

Mutagenesis

Silent mutations were introduced at the amino-acid position 1016 of rSlo1 using two sequential polymerase chain reactions to create a *Xho*I (from CTCGAA to CTCGAG) restriction site. Cassette mutagenesis was performed to delete specific amino-acid sequences. Mutations were generated by polymerase chain reaction using mutagenic primers. Synthetic oligonucleotides were obtained from Cosmo Genetech (Seoul, Korea). The amplified DNA fragments flanked by *Pac*I and *Xho*I were substituted for the WT *rSlo1* gene in pcDNA3.1(+) vector using *Bam*HI and *Xba*I restriction sites. To confirm the DNA sequence of each mutant channel, DNA sequencing was performed using an ABI 377 automatic DNA sequencer (PerkinElmer Life and Analytical Sciences, Waltham, MA).

Electrophysiological recordings and data analysis

Ionic currents carried by WT and mutant rSlo1 channels were recorded in excised membrane patches of CHO-K1 cells with either an inside-out or whole-cell configuration using an Axopatch 200B amplifier (Axon Instruments, Foster, CA). All patch recordings were performed at room temperature 24–48 h after transfection. Pipettes were prepared from thin-walled borosilicate glass (World Precision Instruments, Sarasota, FL) and fire-polished. Macroscopic channel currents were activated by voltage pulses delivered from a holding potential of −100 mV to test potentials ranging from −80 mV to 150 mV in 10-mV increments. When the pipettes were filled with the solutions described below, the input resistances of electrodes for macroscopic currents were 2.5–3.5 MΩ. The average series resistance, ~2.9 MΩ, was used to compensate electronically for the macroscopic recordings. Signals were filtered at 1–2 kHz using a four-pole low-pass Bessel filter, digitized at a rate of 10 kHz using a Digidata 1200 (Axon Instruments), and stored in a personal computer. Commercial software packages such as Clampex 8.1 (Axon Instruments) and Origin 6.1 (MicroCal, Northampton, MA) were used for the acquisition and analysis of macroscopic data.

Solutions for macroscopic ionic-current recording were prepared as previously reported (29,34). Pipette solutions contained 10 mM HEPES, 2 mM EGTA, 116 mM KOH, and 4 mM KCl. The intracellular solution for perfusion to the internal face of excised patches was the same as the pipette solution except for the addition of supplemental $CaCl_2$. To obtain the precise free concentration of intracellular Ca^{2+} ($[Ca^{2+}]_i$), the appropriate amount of total Ca^{2+} to be added to the intracellular solution was calculated using the program MaxChelator (Patton, Thompson et al., 2004). The pH was adjusted to 7.2 with 2-[*N*-morpholino]ethanesulfonic acid.

Surface biotinylation assay

After transfection, the CHO-K1 cells were washed with ice-cooled phosphate-buffered saline and then biotinylated with 1.5 mg/mL Sulfo-NHS-LC-Biotin (Thermo Fisher Scientific, Rockford, IL) for 1 h at 4°C. The cells were washed three times with phosphate-buffered saline and then lysed with 450 μL lysis buffer (40 mM Tris-HCl, 10 mM EDTA, 5 mM EGTA, 150 mM NaCl, 5% glycerol, 1% NP-40, 2 mM Na_3VO_4, 2 mM NaF) with a protease inhibitor cocktail; ~5% of the cell lysate was removed to determine the amount of total protein, and 90% of the cell lysate was incubated with 50 μL of Neutravidin-agarose (50% slurry; Thermo). Then, immunoblot analysis was performed and data were analyzed using a densitometer.

RESULTS

Size variability and sequence diversity of the loop connecting two RCK domains in the cytosolic region of BK_{Ca} channels

Initially, we aligned the amino-acid sequences of the connecting loop between RCK1 and RCK2 in various orthologs of Slo1 using *ClustalX* (35). Sequence alignment revealed that this region is poorly conserved evolutionarily, as noted above, compared with other regions of the channel (Fig. 1 *B*). In NORSp analyses (36,37), an algorithm predicting irregular secondary structures, the connecting loop of rSlo1 was

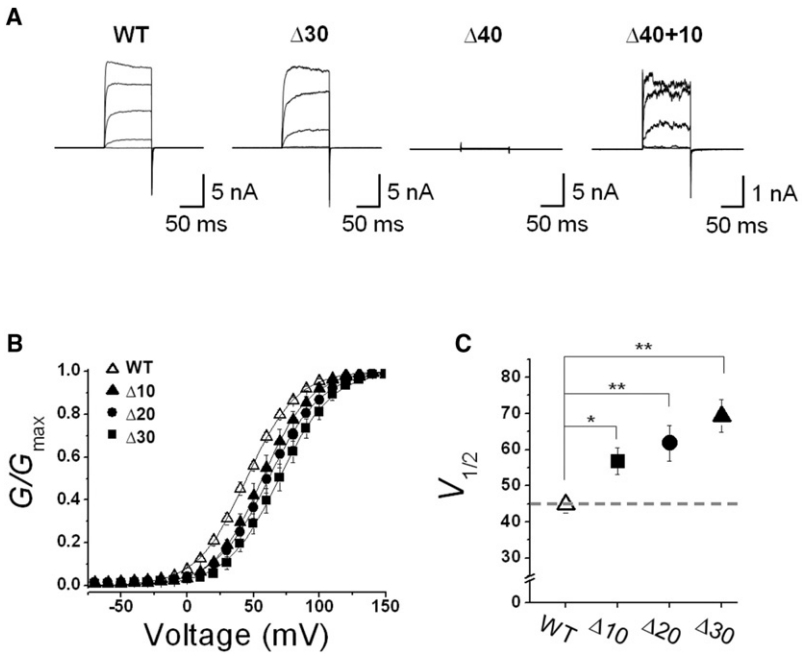

FIGURE 2 Functional effects of deletion mutations with various loop sizes. (*A*) Representative macroscopic current traces of the WT and mutant BK_{Ca} channels. The functional activity of each construct was tested using excised inside-out patch clamp recordings. Ionic currents were induced by voltage steps ranging from −10 mV to 150 mV at 40-mV increments from the holding voltage of −100 mV. (*B*) Normalized conductance-voltage relationships (G/G_{max} versus V_m) from steady-state currents of the WT (*open symbols*) and several mutant channels (*solid symbols*). The membrane was held at −100 mV and then stepped from −10 mV to 150 mV in 10-mV increments for 100 ms. The symbols for each mutant channel are indicated in the inset. Each channel was recorded in the presence of 2 μM $[Ca^{2+}]_i$. Data points were fitted with the Boltzmann function, $G = G_{max} / \{1 + \exp[-zF(V - V_{1/2})/RT]\}$. (*C*) Membrane potential of half-maximal activation ($V_{1/2}$) determined at 2 μM $[Ca^{2+}]_i$. Each data point represents the mean ± SE. Values that differ from the WT by a paired Student's *t*-test at $p < 0.05$ (*) or $p < 0.01$ (**) are indicated.

predicted to be NORS. It is worth mentioning that prokaryotic Ca^{2+}-activated K^+ channels, such as MthK, lack connecting loops in their gating rings. These channel proteins contain only a single RCK domain at the cytosolic C-terminus following the TM domains. Although four RCK domains are provided by each channel subunit, the other four RCK domains are expressed as soluble proteins by an alternative translational initiation and assembled separately to form a homooctameric gating ring (21,30).

It is known that multiple alternatively spliced variants are generated in these NORS regions, resulting in a variety of lengths at the connecting loops (38). When we searched the cytosolic regions of BK_{Ca} channel orthologs from sea urchin to human, we found that the connecting loop between RCK1 and RCK2 varies in length from ~100 to 240 amino acids. Intriguingly, none of the BK_{Ca} channel isoforms showed a loop size smaller than 101 amino acids (Fig. 1 *C*). We therefore wondered whether the length of the connecting loop plays any functional role in channel activity, and whether there is an upper and/or lower limit to the loop size.

Minimum size requirement of the connecting loop revealed by serial deletions

We first sought to determine whether the length of the NORS region connecting the two RCK domains is important for the function of the BK_{Ca} channel. To answer this question, we generated a series of deletion mutants in which the NORS region of the BK_{Ca} channels was shortened by 10–90 amino acids at the center of the loop (see Fig. S1 in the Supporting Material). The WT channel and each mutant were expressed in CHO-K1 cells, and their functional activities were analyzed. Shown in Fig. 2 *A* are the ionic currents recorded in the presence of 2 μM $[Ca^{2+}]_i$ for WT and mutant rat Slo1 channels in excised inside-out membrane patches. Although deletion within the NORS segment of 10, 20, or 30 amino acids resulted in functional BK_{Ca} channels and generated macroscopic channel currents, mutant channels containing deletions >40 amino acids produced no ionic currents in response to either membrane depolarization or increased intracellular Ca^{2+}. When we inserted a 10-amino acid of random sequence (GSSGDGSAAG) into the 40-amino acid deletion (Δ40+10), we were able to rescue the macroscopic channel currents (Fig. 2 *A*, *right panel*). This result suggests that a minimum length of ~70 amino acids in the connecting loop is required for the channel to be functional.

When we analyzed the deletion mutants that evoked macroscopic ionic currents, we observed that these channels were activated at progressively more positive voltages as the size of deletion increased from 10 to 30 amino acids (Fig. 2 *A*). We quantified the effects of the loop deletions on the voltage-dependent activation of the channel by plotting the conductance-voltage (*G-V*) relationships of the WT (Fig. 2 *B*, *open symbols*) and the mutants (*solid symbols*). Whereas the WT channels were activated with the half-maximum voltage ($V_{1/2}$) of 44.8 ± 2.3 mV, the $V_{1/2}$ values of the deletion mutants, Δ10, Δ20, and Δ30, were estimated as 56.8 ± 3.7 mV, 61.8 ± 5.0 mV, and 69.4 ± 4.6 mV, respectively. Intriguingly enough, the $V_{1/2}$ values showed a near-linear relationship against the numbers of amino acid deleted (Fig. 2 *C*) and the total length of the NORS segment (see Fig. 7). These results indicate that shortening the connecting loop progressively shifted the voltage-dependent activation curve to the positive voltage range, and suggest that the NORS segment in between two RCK domains influences the gating equilibrium of the channel.

Since we were not able to record any ionic currents from the mutant channels containing deletions >40 residues, we wondered whether those channels were properly translated and adequately expressed on the surface membrane. We examined the protein expression and the surface targeting of the WT channel and three different deletion mutants (Δ30, Δ50, and Δ70) using Western blot and surface biotinylation analyses, as shown in Fig. 3. The results showed that all three deletion mutants were expressed well and targeted acceptably to the cell surface compared with the WT. Thus, the lack of ionic currents in Δ50 and Δ70 mutants cannot be attributed to a failure of translation or improper targeting to the cell surface.

Positional effects of 30-residue deletions within the connecting loop

We next investigated the functional significance of specific regions of the loop by producing seven overlapping 30-amino acid deletions at various sites within the loop (Δ30_1–Δ30_7) (Fig. 4 *A*). When we expressed the deletion mutants and recorded the ionic currents evoked by each mutant channel, we found that deletions in different regions produced various effects on the level of current expression (Fig. S2). Although five of the seven deletion mutants, Δ30_2–Δ30_6, produced potassium currents activated by both membrane depolarization and intracellular Ca^{2+}, the two deletions at the most peripheral ends of the loop, Δ30_1 and Δ30_7, failed to generate any ionic currents. Among the five functional mutant channels, the three central deletion mutants, Δ30_3, Δ30_4, and Δ30_5, evoked robust currents suitable for excised inside-out patch recordings. As shown in Fig. 4 *B*, the ionic currents of the deletion mutants were activated at more positive voltages than those of the WT channel. In Fig. 4 *C*, the *G-V* relationships of the WT (*open symbols*) and three different mutant channels (*solid symbols*) are compared. The *G-V* curves of all three mutants were shifted in a positive direction and the $V_{1/2}$ values of Δ30_3, Δ30_4, and Δ30_5 were determined to be 70.5 ± 3.7, 68.1 ± 2.1, 69.4 ± 4.6 mV, respectively (Fig. 3, *C* and *D*). The similarity in the pattern of *G-V* curve shifts brought about by these 30-residue deletions at the central region of the loop indicates that the length, rather than the specific sequence of the loop, affects the channel gating at this part of the loop.

Since the two adjacent mutants, Δ30_2 and Δ30_6, produced much smaller currents, we had to utilize whole-cell configuration to record the channel currents (Fig. S3 *A*). The *G-V* curves of the two mutant channels were compared with that of the WT channel, and Δ40+10 was also recorded in whole-cell mode in the presence of 2 μM Ca^{2+} (Fig. S3, *B and C*). The two mutant channels, Δ30_2 and Δ30_6, exhibited greater shifts in their *G-V* curves toward the positive direction (108.9 ± 7.1 mV and 92.5 ± 10.4 mV, respectively) compared to the three different deletions at the central part of the loop (Δ30_3, Δ30_4, and Δ30_5). These results indicate that the loop regions covered by Δ30_2 and Δ30_6 affect the functionality of the channel in at least two different aspects: the level of current expression and the voltage dependence.

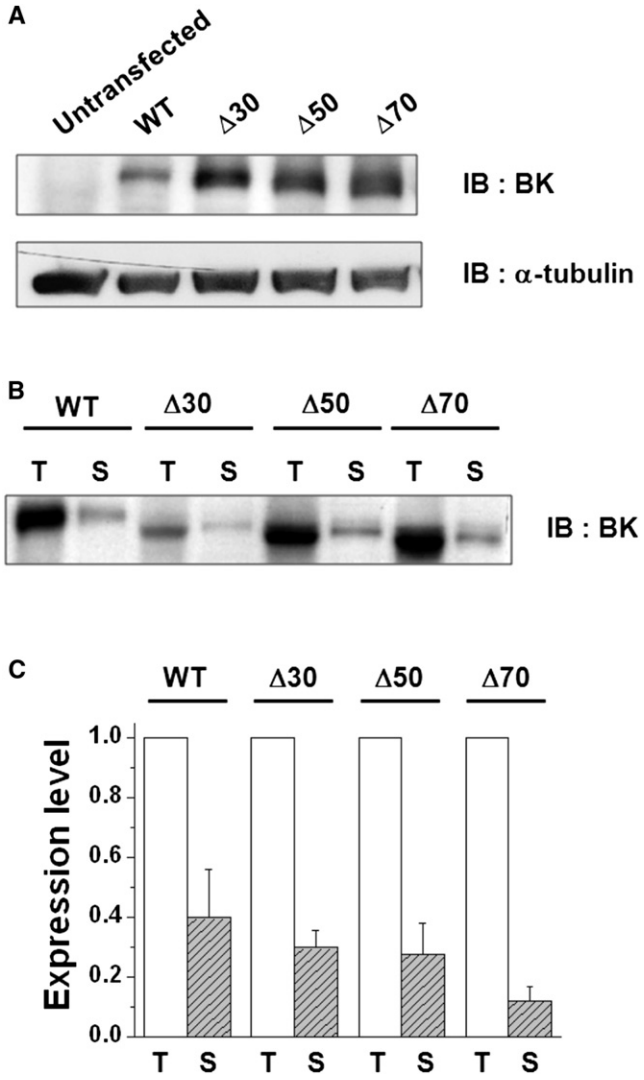

FIGURE 3 Cell-surface expression of WT and three different mutant channels. (*A*) Immunoblot analysis of the WT and NORS deletion mutants. The WT and three different mutant channels (Δ30, Δ50, and Δ70) were transiently transfected in CHO-K1 cells and the cell lysates were subjected to immunoblot (IB) analysis using anti-BK_{Ca} channel antibody (α-BK) and antitubulin antibody (α-tubulin), respectively. (*B*) Cell-surface biotinylation of WT and NORS deletion mutants. Cells transfected with the WT and deletion mutants were biotinylated and subsequently precipitated using Neutravidin-agarose. The precipitates were subjected to immunoblot analysis. Total protein (T) and surface-expressed BK_{Ca} channel (S) are shown. (*C*) Densitometric quantitation of T and S. Immunoreactive band intensities of the WT and mutant channels were quantified with a densitometer. The band intensity of the channel expressed on the cell surface (S, *hatched bars*) was normalized by that of the total channel (T, *open bars*). Data represent the mean ± SE ($n = 4$). No significant changes in surface expression were detected among mutant channels (paired *t*-test).

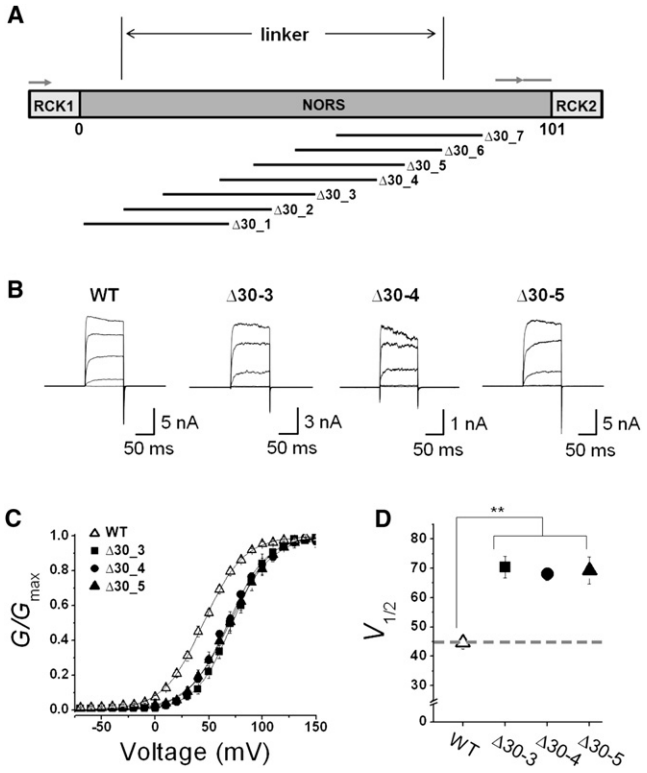

FIGURE 4 Functional effects of 30-amino acid deletions at different positions. (*A*) Relative position of 30-amino acid deletion generated in the loop region connecting RCK1 and RCK2. The position of each deletion is shown in Fig. S2. (*B*) Representative macroscopic current traces of the WT and mutant BK_{Ca} channels. The functional activity of each construct was tested using excised inside-out patch clamp recordings. Ionic currents were induced by voltage steps ranging from −10 mV to 150 mV at 40 mV increments from the holding voltage of −100 mV. Due to the marked differences in channel expression level, the scale bar for each mutant channel was adjusted accordingly. (*C*) Normalized conductance-voltage relationships (G/G_{max} versus V_m) of the WT (*open symbols*) and several mutant channels (*solid symbols*). The membrane was held at −100 mV and then stepped from −80 mV to 150 mV in 10-mV increments for 100 ms. The symbols for each mutant channel are indicated in the inset. Each channel was recorded in the presence of 2 μM $[Ca^{2+}]_i$. Data points were fitted with the Boltzmann function. (*D*) Membrane potential of half-maximal activation ($V_{1/2}$) determined at 2 μM $[Ca^{2+}]_i$. Each data point represents the mean ± SE. Values that differ from the WT by a paired Student's *t*-test at $p < 0.05$ (*) or $p < 0.01$ (**) are indicated.

It is also worth noting that the two deletions at the N- and C-terminal ends of the loop, Δ30_1 and Δ30_7, failed to generate any ionic currents. Because the ends of the loop are connected to RCK1 and RCK2, respectively, the most proximal regions of the loop may interact with or participate in these RCK domains and play an important role in Ca^{2+}-dependent gating of the channel. This proposition is buttressed by the fact that the amino-acid sequence in these regions of the loop is more highly conserved among the BK_{Ca} channel orthologs than the rest of the NORS region (Fig. 1). Thus, we may have to reset the boundary of the flexible connecting loop between two RCK domains to the region covering the N-terminal end of Δ30_2 to the C-terminal end of Δ30_5 (Fig. 4 *A*).

Structural tension on the loop is relieved by coexpression of "core" and "tail" regions

To determine whether the reduced channel activity that results from shortening the NORS is caused by structural constraints within the gating ring, we coexpressed two separable domains with a 30-amino acid deletion within the loop: the ''core'' domain that contains the entire upstream region of the channel from the N-terminal end to the deletion site within the connecting loop, and the ''tail'' domain that bears the region downstream of that site to the C-terminal end. In previous studies, investigators showed that they could assemble functional BK_{Ca} channels by coexpressing the ''core'' region and the ''tail'' region as two separate polypeptides (12–14). We hypothesized that the coexpression of our deletion mutants would effectively dissect the loop and thus release any structural tension caused by the deletion.

Whereas the expression of either the core or tail alone generated no detectable currents, even under large depolarization or high $[Ca^{2+}]_i$, coexpression of the ''core'' domain with either of the two different ''tails'' containing a 30-residue deletion (core+tailΔ30-5 and core+tailΔ30-6) produced robust ionic currents (Fig. 5 *A*). Remarkably enough, the coexpression of the core and tails of the deletion mutant (core+tailΔ30) showed a *G-V* relationship (46.1 ± 2.9 mV for core+tailΔ30-4 and 44.3 ± 3.6 mV for core+tailΔ30-5) very similar to that of the WT channel (44.8 ± 2.3 mV), despite the deletions in the NORS region (Fig. 5 *B*). We also performed a similar experiment with the nonfunctional Δ40 mutant to determine whether coexpression of the separable domains could recover its functionality. Although the channel activity was completely abolished by the 40-residue deletion of the whole channel, coexpression of the core region and the tail domains containing the 40-residue deletion restored channel functionality (Fig. 5 *A*, *right panel*). Moreover, the *G-V* relationship of the coexpressed core and the Δ40-tail (core+tailΔ40) was shown to be very similar to that of the WT channel, strongly suggesting that the removal of structural tension caused by the shortened NORS resulted in an almost full recovery of channel activity (Fig. 5 *C*; see also Fig. 7). These results further support the idea that shortening the loop between the two RCK domains provides structural constraints for the gating machinery.

Lack of effects on channel function by insertional substitution

As shown in Fig. 1 *B*, many BK_{Ca} channel variants have loops connecting RCK1 and RCK2 domains that are significantly longer than 101 residues. We thus wondered whether increased loop size has any effects on channel function. Since both proximal regions of the loop were shown to be functionally important (Fig. 4), we decided to replace the central residues Leu^{672}-Lys^{723} with the corresponding NORS region of *Drosophila* Slo (dSlo) or BK_{Ca} channel α-subunit, Arg^{648}-Met^{798} (39). This replacement was done

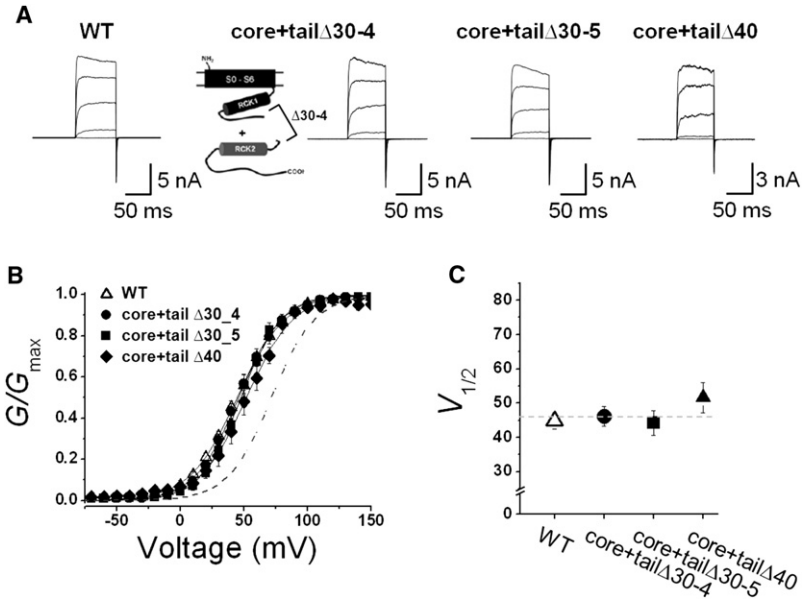

FIGURE 5 Coexpression of two separable domains with 30-amino acid deletions of NORS. (*A*) Representative macroscopic current traces of the WT and mutant BK_{Ca} channels. Schematic of coexpression of two separable domains with the deletion of Δ30-4 position is represented. The functional activity of each construct was tested using excised inside-out patch clamp recordings. Ionic currents were induced by voltage steps ranging from −10 mV to 150 mV at 40 mV increments from the holding voltage of −100 mV. (*B*) Normalized conductance-voltage relationships (G/G_{max} versus V_m) of the WT (*open symbols*) and several mutant channels (*solid symbols*). The membrane was held at −100 mV and then stepped from −80 mV to 150 mV in 10 mV increments for 100 ms. The symbols for each mutant channel are indicated in the inset. Each channel was recorded with 2 μM $[Ca^{2+}]_i$. Data points were fitted with the Boltzmann function. (*C*) Membrane potential of half-maximal activation ($V_{1/2}$) determined at 2 μM $[Ca^{2+}]_i$. Each data point represents the mean ± SE. Values that differ from the WT by a paired Student's *t*-test at $p < 0.05$ (*) or $p < 0.01$ (**) are indicated.

to increase the length of the loop by 62 residues. We then examined the functional activity of the insertional mutant (+62) (Fig. 6 *A*). Although the loop segment lengthened significantly, this mutant channel showed a *G-V* relationship virtually identical to that of the WT channel (Fig. 6, *B* and *C*). Thus, although shortening the connecting loop decreases channel activity, lengthening the loop has no apparent effects on channel functionality. These results further confirm that the specific sequence of the connecting loop region is not important for channel function, and strongly suggest that this region acts as a flexible linker connecting two RCK domains.

DISCUSSION

In our previous studies (28,33), we delineated two RCK domains (RCK1 and RCK2) in the cytosolic domain of the BK_{Ca} channel carboxyl terminus and demonstrated the functional importance of these domains via two different interfaces. These two RCK domains are connected by a loop of

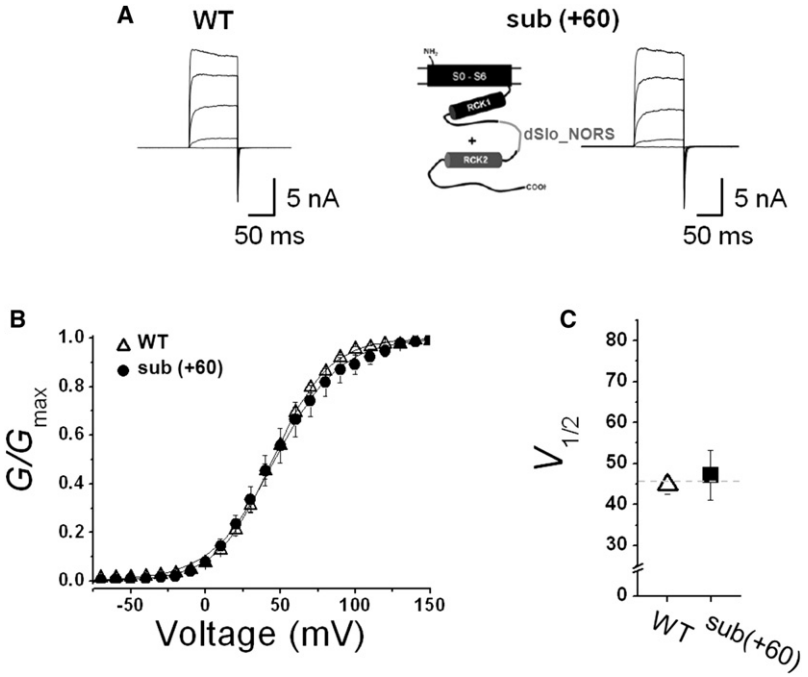

FIGURE 6 Functional effects of an insertional substitution. (*A*) Representative macroscopic current traces of the WT and mutant BK_{Ca} channels. Schematic of the substitution of the NORS region with the loopy sequence from dSlo (dSlo_NORS) is represented. The functional activity of the construct was tested using excised inside-out patch clamp recordings. Ionic currents were induced by voltage steps ranging from −10 mV to 150 mV at 40 mV increments from the holding voltage of −100 mV. (*B*) Normalized conductance-voltage relationships (G/G_{max} versus V_m) of the WT (*open symbols*) and the mutant channel (*solid symbols*). The membrane was held at −100 mV and then stepped from −80 mV to 150 mV in 10 mV increments for 100 ms. The symbols for the mutant channel are indicated in the inset. Each channel was recorded with 2 μM $[Ca^{2+}]_i$. Data points were fitted with the Boltzmann function. (*C*) Membrane potential of half-maximal activation ($V_{1/2}$) determined at 2 μM $[Ca^{2+}]_i$. Each data point represents the mean ± SE. Values that differ from the WT by a paired Student's *t*-test at $p < 0.05$ (*) or $p < 0.01$ (**) are indicated.

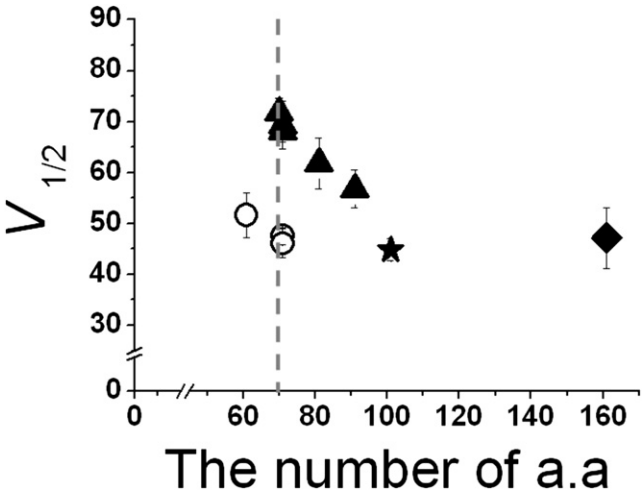

FIGURE 7 Summary of mutational analyses in NORS connecting two RCK domains. Membrane potential of half-maximal activation ($V_{1/2}$) at 2 μM $[Ca^{2+}]_i$ was plotted against the number of amino acids comprising the loop connecting RCK1 and RCK2 domains (NORS). Symbols represent the rat Slo1 WT (101 residue, *solid star*), deletion mutants of various sizes (*solid triangles*), deletion mutants coexpressed as two separable proteins of the core and the tails containing corresponding deletion (*open circles*), and an insertion mutant (*solid square*). Each data point represents the mean ± SE.

various lengths in diverse BK_{Ca} channel orthologs that is predicted to be nonstructural. Intrigued by the fact that none of these loops are smaller than 101 amino acids in length, we performed a series of deletion mutations to examine the functional significance of the loop.

Our results showed that the position of the *G-V* relationship shifted progressively in the positive direction as the loop was shortened by 10–30 residues (Fig. 7, *solid triangles*), as if the apparent equilibrium between closed and open states shifted toward the closed states. The stabilizing effect on the closed state can be estimated at ~8.5 mV (or ~0.15 kcal/mol) per 10-residue deletion. It remains to be examined, however, whether the deletions of the loop affect other aspects of the channel, such as the affinity of the Ca^{2+} or coupling of Ca^{2+} binding to channel opening. We also found that the extent of the $V_{1/2}$ shift was independent of the position of the deletions, as long as they were not too close to the flanking RCK domains. A deletion of >40 residues or a loop size of <60 residues resulted in a nonfunctional channel (Fig. 7, *dotted vertical line*). It seems clear that the smaller loop size does not influence the protein expression or the surface targeting of the channel protein significantly. It is not clear at this point whether this lower size limit of the loop represents the minimum length for the two RCK domains to assemble into the heterooctameric ''gating ring'', as proposed for the BK_{Ca} channel in previous studies (21,30). It is evident, however, that not only can the experimental dissection of the nonfunctional mutant at the loop rescue the channel functionality, it can also restore the *G-V* relationship to that of the WT channel (Fig. 7, *open circles*). These results strongly suggest that the shifts in the *G-V* relationship resulted from tension in the loop. On the other hand, increasing the size of the loop did not exhibit any functional effects on channel gating. When we substituted the loop with the corresponding region from the *Drosophila* BK_{Ca} channel resulting in a 62-residue insertion, the *G-V* relationships of both the WT and the insertional mutant channel were virtually identical (Fig. 7, *solid square*).

Here, we propose that the change in functionality of the mutants is due to increased strain on the connecting loop between the two RCK domains. In analogy to the MthK channel, one can imagine that BK_{Ca} channels have a gating ring comprised of RCK domains with alternating assembly and flexible interfaces (21,30,32). The relative movement of the flexible interface has been shown to be the main conformational change induced by Ca^{2+} binding in MthK. It has also been suggested that the dimeric pairs of RCK domains on a single subunit are responsible for cooperative activation of BK_{Ca} channels by calcium (40). Based on our functional results and previous structural studies (21,30, 41), we can hypothesize that applying tension to the loop region connecting the two RCK domains restricts the movement of the flexible interface, and this restriction stabilizes the closed conformation of the channel, leading to decreased open probability of the channel. Thus, it is conceivable that the interface formed between two RCK domains linked by a NORS in the same subunit would be flexible.

The physiological role of the loop connecting RCK1 and RCK2 remains unclear. In major splicing variants of mammalian BK_{Ca} channels, the connecting loops contain 101 amino acid residues (Fig. 7, *solid star*). These loops seem to be long enough to not experience increased tension during normal channel activity. However, we can imagine that the loop is of the appropriate length to respond to any fluctuation in tension and to affect channel function accordingly. It will be intriguing to explore this possibility further; for example, such activity could be used to identify a binding protein that interacts with the loop region and modulates the *G-V* relationship of the channel by temporarily altering loop tension.

In summary, we show that the activity of the BK_{Ca} channel can be altered by changing the length of the loop connecting two RCK domains, and propose that the channel function can be modulated by adjusting the tension of this loop region.

SUPPORTING MATERIAL

Three figures are available at http://www.biophysj.org/biophysj/supplemental/S0006-3495(09)01023-6.

We thank the members of the Laboratory of Molecular Neurobiology, Gwangju Institute of Science and Technology, for their valuable comments and timely help throughout the work presented here.

This research was supported by grants from the Korea Science and Engineering Foundation (R01-2006-000-10880-0 and R11-2007-007-02002-0) and the Korea Research Foundation (E00025) to C.-S. Park.

REFERENCES

1. Vergara, C., R. Latorre, N. V. Marrion, and J. P. Adelman. 1998. Calcium-activated potassium channels. *Curr. Opin. Neurobiol.* 8:321–329.
2. Ghatta, S., D. Nimmagadda, X. Xu, and S. T. O'Rourke. 2006. Large-conductance, calcium-activated potassium channels: structural and functional implications. *Pharmacol. Ther.* 110:103–116.
3. Latorre, R., and S. Brauchi. 2006. Large conductance Ca^{2+}-activated K^+ (BK) channel: activation by Ca^{2+} and voltage. *Biol. Res.* 39:385–401.
4. Cui, J., D. H. Cox, and R. W. Aldrich. 1997. Intrinsic voltage dependence and Ca^{2+} regulation of *mslo* large conductance Ca^{2+}-activated K^+ channels. *J. Gen. Physiol.* 109:647–673.
5. Zhang, X., C. R. Solaro, and C. J. Lingle. 2001. Allosteric regulation of BK channel gating by Ca^{2+} and Mg^{2+} through a nonselective, low affinity divalent cation site. *J. Gen. Physiol.* 118:607–636.
6. Robitaille, R., M. L. Garcia, G. J. Kaczorowski, and M. P. Charlton. 1993. Functional colocalization of calcium and calcium-gated potassium channels in control of transmitter release. *Neuron.* 11:645–655.
7. Nelson, M. T., H. Cheng, M. Rubart, L. F. Santana, A. D. Bonev, et al. 1995. Relaxation of arterial smooth muscle by calcium sparks. *Science.* 270:633–637.
8. Yazejian, B., D. A. DiGregorio, J. L. Vergara, R. E. Poage, S. D. Meriney, et al. 1997. Direct measurements of presynaptic calcium and calcium-activated potassium currents regulating neurotransmitter release at cultured. *Xenopus* nerve-muscle synapses. *J. Neurosci.* 17:2990–3001.
9. Duncan, R. K., and P. A. Fuchs. 2003. Variation in large-conductance, calcium-activated potassium channels from hair cells along the chicken basilar papilla. *J. Physiol.* 547:357–371.
10. Ahluwalia, J., A. Tinker, L. H. Clapp, M. R. Duchen, A. Y. Abramov, et al. 2004. The large-conductance Ca^{2+}-activated K^+ channel is essential for innate immunity. *Nature.* 427:853–858.
11. Lu, R., A. Alioua, Y. Kumar, M. Eqhbali, E. Stefani, et al. 2006. MaxiK channel partners: physiological impact. *J. Physiol.* 570:65–72.
12. Toro, L., M. Wallner, P. Meera, and Y. Tanaka. 1998. Maxi-K_{Ca}, a unique member of the voltage-gated K channel superfamily. *News Physiol. Sci.* 13:112–117.
13. Wei, A., C. Solaro, C. Lingle, and L. Salkoff. 1994. Calcium sensitivity of BK-type K_{Ca} channels determined by a separable domain. *Neuron.* 13:671–681.
14. Schreiber, M., and L. Salkoff. 1997. A novel calcium-sensing domain in the BK channel. *Biophys. J.* 73:1355–1363.
15. Schreiber, M., A. Yuan, and L. Salkoff. 1999. Transplantable sites confer calcium sensitivity to BK channels. *Nat. Neurosci.* 2:416–421.
16. Horn, R. 2002. Coupled movements in voltage-gated ion channels. *J. Gen. Physiol.* 120:449–453.
17. Gandhi, C. S., and E. Y. Isacoff. 2002. Molecular models of voltage sensing. *J. Gen. Physiol.* 120:455–463.
18. Bezanilla, F. 2002. Voltage sensor movements. *J. Gen. Physiol.* 120:465–473.
19. Diaz, L., P. Meera, J. Amigo, E. Stefani, O. Alvarez, et al. 1998. Role of the S4 segment in a voltage-dependent calcium-sensitive potassium (hSlo) channel. *J. Biol. Chem.* 273:32430–32436.
20. Ma, Z., X. J. Lou, and F. T. Horrigan. 2006. Role of charged residues in the S1–S4 voltage sensor of BK channels. *J. Gen. Physiol.* 127: 309–328.
21. Jiang, Y., A. Pico, M. Cadene, B. T. Chait, and R. MacKinnon. 2001. Structure of the RCK domain from the *E. coli* K^+ channel and demonstration of its presence in the human BK channel. *Neuron.* 29:593–601.
22. Jiang, Y., A. Lee, J. Chen, M. Cadene, B. T. Chait, et al. 2002. Crystal structure and mechanism of a calcium-gated potassium channel. *Nature.* 417:515–522.
23. Pico, A. 2003. RCK domain model of calcium activation in BK channels. PhD thesis. The Rockefeller University, New York.
24. Reference deleted in proof.
25. Bao, L., A. M. Rapin, E. C. Holmstrand, and D. H. Cox. 2002. Elimination of the BK_{Ca} channel's high-affinity Ca^{2+} sensitivity. *J. Gen. Physiol.* 120:173–189.
26. Shi, J., G. Krishnamoorthy, Y. Yang, L. Hu, N. Chaturvedi, et al. 2002. Mechanism of magnesium activation of calcium-activated potassium channels. *Nature.* 418:876–880.
27. Xia, X. M., X. Zeng, and C. J. Lingle. 2002. Multiple regulatory sites in large-conductance calcium-activated potassium channels. *Nature.* 418:880–884.
28. Roosild, T. P., K. T. Le, and S. Choe. 2004. Cytoplasmic gatekeepers of K1-channel flux: a structural perspective. *Trends Biochem. Sci.* 29: 39–45.
29. Kim, H. J., H. H. Lim, S. H. Rho, S. H. Eom, and C. S. Park. 2006. Hydrophobic Interface between two regulators of K^+ conductance domains critical for calcium-dependent activation of large conductance Ca^{2+}-activated K^+ channels. *J. Biol. Chem.* 281:38573–38581.
30. Yusifov, T., N. Savalli, C. S. Gandhi, M. Ottolia, and R. Olcese. 2008. The RCK2 domain of the human BK_{Ca} channel is a calcium sensor. *Proc. Natl. Acad. Sci. USA.* 105:376–381.
31. Ye, S., Y. Li, L. Chen, and Y. Jiang. 2006. Crystal structures of a ligand-free MthK gating ring: insights into the ligand gating mechanism of K^+ channels. *Cell.* 126:1161–1173.
32. Niu, X., X. Qian, and K. L. Magleby. 2004. Linker-gating ring complex as passive spring and Ca^{2+}-dependent machine for a voltage- and Ca^{2+}-activated potassium channel. *Neuron.* 42:745–756.
33. Lingle, C. J. 2007. Gating rings formed by RCK domains: keys to gate opening. *J. Gen. Physiol.* 129:101–107.
34. Kim, H. J., H. H. Lim, S. H. Rho, L. Bao, J. H. Lee, et al. 2008. Modulation of the conductance-voltage relationship of the BK_{Ca} channel by mutations at the putative flexible interface between two RCK domains. *Biophys. J.* 94:446–456.
35. Ha, T. S., S. Y. Jeong, S. W. Cho, H. Jeon, G. S. Roh, et al. 2000. Functional characteristics of two BK_{Ca} channel variants differentially expressed in rat brain tissues. *Eur. J. Biochem.* 267:910–918.
36. Thompson, J. D., T. J. Gibson, F. Plewniak, F. Jeanmougin, and D. G. Higgins. 1997. The CLUSTAL_X windows interface: flexible strategies for multiple sequence alignment aided by quality analysis tools. *Nucleic Acids Res.* 25:4876–4882.
37. Liu, J., H. Tan, and B. Rost. 2002. Loopy proteins appear conserved in evolution. *J. Mol. Biol.* 322:53–64.
38. Liu, J., and B. Rost. 2003. NORSp: predictions of long regions without regular secondary structure. *Nucleic Acids Res.* 31:3833–3835.
39. Shiptson, M. J. 2001. Alternative splicing of potassium channels: a dynamic switch of cellular excitability. *Trends Cell Biol.* 11:353–358.
40. Atkinson, N. S., G. A. Robertson, and B. Ganetzky. 1991. A component of calcium-activated potassium channels encoded by the *Drosophila slo* locus. *Science.* 253:551–555.
41. Qian, X., X. Niu, and K. L. Magleby. 2006. Intra- and intersubunit cooperativity in activation of BK channels by Ca^{2+}. *J. Gen. Physiol.* 128:389–404.